Transport of Deposited Atoms throughout Strain-Mediated Self-Assembly

Oussama Moutanabbir,[1,2,*] Satoru Miyamoto,[1] Eugene E. Haller,[3,4] and Kohei M. Itoh[1]

[1]*School of Fundamental Science and Technology, Keio University, 3-14-1 Hiyoshi, Kohoku-ku, Yokohama 223-8522, Japan*
[2]*Max Planck Institute of Microstructure Physics, Weinberg 2, Halle (Saale), 06120 Germany*
[3]*Department of Materials Science and Engineering, University of California, Berkeley, Berkeley, California 94720-1760, USA*
[4]*Lawrence Berkeley National Laboratory, 1 Cyclotron Road, Berkeley, California 94720, USA*
(Received 10 January 2010; published 6 July 2010)

Using enriched isotopes, we developed a method to elucidate the long-standing issue of Ge transport governing the strain-driven self-assembly. Here ^{76}Ge was employed to form the 2D metastable layer on a Si(001) surface, while the 3D transition and growth were completed by additional evaporation of ^{70}Ge. This isotope tracing combined with the analysis of the Ge-Ge LO phonon enables the tracking of the origin of Ge atoms and their flow towards the growing islands. This atomic transport was quantified based on the quasiharmonic approximation of Ge-Ge vibrations and described using a rate equation model.

DOI: 10.1103/PhysRevLett.105.026101 PACS numbers: 68.55.A−, 68.43.Jk, 81.07.Ta, 28.60.+s

The elastic energy stored during lattice-mismatched heteroepitaxy can be relieved by surface roughening, step bunching, dislocation formation, and assembly of 3D nanostructures [1,2]. Considerable effort has been expended to understand the atomic processes involved in these morphological instabilities, aiming at suppressing or exploiting them [3–7]. In particular, the phenomenon of self-assembly has been the subject of intensive investigations as a powerful nanofabrication tool by which a variety of defect-free semiconductor quantum dots and nanowires can be prepared, inspiring a wide spectrum of potential nanoscale technologies [3]. The formation of these nanostructures occurs in the Stranski-Krastanow growth mode. In this mode, the deposited atoms first form a 2D metastable layer. The onset of the nucleation and growth of 3D structures take place when this 2D layer reaches a critical thickness. This instability of the planar growth depends strongly on the misfit strain, which increases progressively as a result of the surface segregation [8,9]. This 2D-3D transition and island growth are exclusively governed by surface diffusion processes [10].

Experimental observations have provided clear evidence that the 2D layer transfers material collectively to 3D nanostructures during growth and annealing [11–21]. Nevertheless, the chemical and structural probes used in these investigations cannot discriminate between atoms deposited during the initial 2D growth and those deposited after the onset of the 3D growth. These two groups of atoms are, however, distinct as they follow different pathways prior to their incorporation into the growing islands. Thus the elucidation of the contribution of each group to the growth is critical to the understanding of the physics of heteroepitaxy and strain-mediated self-assembly. Here we believe that we unveiled key mechanisms underlying the transport of deposited atoms in the Ge/Si system. Through stable isotope tracing, we were able to distinguish between the two aforementioned groups of atoms. The flow of Ge and the contribution of each group to the 3D growth are quantified based on the quasiharmonic approximation of Ge-Ge vibrations.

The growth was performed on a *p*-type Si(001) substrate in a solid source molecular beam epitaxy system at $T = 620\,^{\circ}$C. Two Ge enriched isotope sources were employed in a two-isotope growth process. Figure 1(a) illustrates this process in the abrupt epitaxy configuration. In this approach, the planar layer is grown by deposition of ^{76}Ge-rich material (85.1%^{76}Ge + 14.5%^{74}Ge), and the 2D-3D transition and growth of islands are achieved by the immediate evaporation of ^{70}Ge-rich material (96.3%^{70}Ge + 2.1%^{72}Ge). For convenience, in the text we refer to the sources used as ^{70}Ge and ^{76}Ge. Figure 1(b) displays the Ge-Ge LO phonon of the two crystals used in the growth. As expected from the difference in the average mass, the two Ge-Ge modes are $\sim$11.8 cm^{-1} away from each other. This dependence of phonon frequencies on the

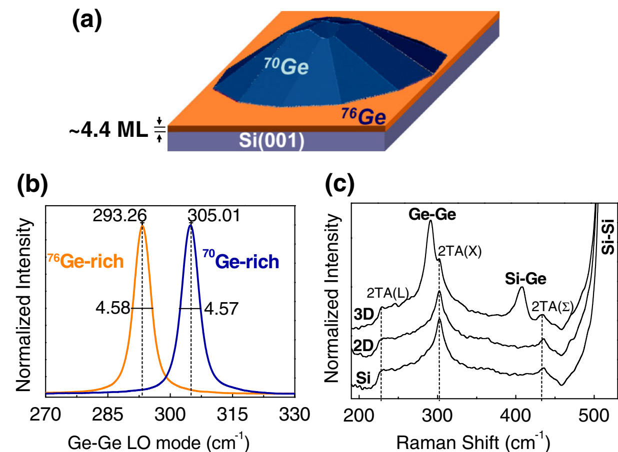

FIG. 1 (color online). (a) Schematic illustration in the abrupt configuration of the two-isotope growth of a Ge/Si(001) island. (b) Ge-Ge modes of ^{70}Ge and ^{76}Ge sources used in this study. (c) Raman spectra of Si(001) bare substrate (Si), 4.4 ML of ^{76}Ge deposited on Si(001) (2D), and a ^{76}Ge 3D island grown by depositing 1 ML of ^{76}Ge on the 2D layer (3D).

 © 2010 The American Physical Society

isotopic content can be described by the quasiharmonic analysis within the virtual crystal approximation [22], which gives $\omega \propto m^{-1/2}$, where ω is the phonon frequency and m is the average mass. Here the description of vibrations neglects third and higher order derivatives of the crystalline potential, which is a valid approximation in semiconductors at room temperature (RT).

The Ge deposition rate was fixed at $\rho = 0.04$ ML/s for the two sources. The substrate was cooled down to room temperature immediately after the growth. The surface morphology was investigated by *ex situ* atomic force microscopy (AFM) in the tapping mode. The critical thickness of the 2D-3D transition was defined as the maximum ^{76}Ge coverage at which no 3D islands are observable by AFM. Under our growth conditions, this thickness is found to be $\theta_0 = (4.4 \pm 0.1)$ ML. A similar critical thickness ($\sim$4.2 ML) was reported recently by Brehm *et al.* [23]. For an additional amount of ^{70}Ge$(\theta) \geq 1$ ML, no new nucleation events are detected. The morphology of the grown islands is identical to the system described in Ref. [21]. Raman scattering spectroscopy was carried out at RT in backscattering geometry using a 514.5 nm Ar^+ laser focused on a 1-μm-diameter spot.

As shown in Fig. 1(c), the 2D layer has no clear Raman signal; hence the spectra of the analyzed samples contain only the contributions from the islands and the underlying Si substrate as demonstrated earlier [24]. Therefore, the island intrinsic Raman modes can be extracted by subtracting the Si substrate background signal from the raw signal [24]. Note that the intrinsic Raman signal is also sensitive to strain and Si content in the island [24,25]. Thus to differentiate the contribution of the isotope composition from the other parameters influencing phonon frequencies, two sets of reference samples were grown under the same experimental conditions using monoisotopic beams ^{70}Ge and ^{76}Ge in a single isotope evaporation. At a fixed coverage, the morphology, amount of strain, and Si content are identical in the three sets of samples. In this way, the relative Raman peak positions can be directly associated with the isotopic composition. Based on the aforementioned quasiharmonic approximation, the fraction of ^{76}Ge atoms within the growing ^{70}Ge/^{76}Ge island, $y(\theta)$, can be directly estimated from $(\omega_{70/76}/\omega_{\text{ref}})^2$, where $\omega_{70/76}$ and ω_{ref} are the Ge-Ge wave numbers in the ^{70}Ge/^{76}Ge islands and in the corresponding monoisotopic islands at the same θ, respectively. A slight deviation from this approximation is expected for isotopically disordered materials. The mass disorder-induced frequency shift in the Ge-Ge LO phonon reaches a maximum of $\sim$1.06 cm^{-1} at 10 K in ^{70}Ge$_{0.5}$^{76}Ge$_{0.5}$ crystal, representing the largest isotope disorder in Ge [26]. However, considering that our measurements were carried out at RT with a spectral resolution of $\sim$0.6 cm^{-1}, this isotope disorder cannot affect our analysis.

Because of the overlap with the 2 TA(X) phonon of Si substrate at $\sim$300 cm^{-1}, meaningful intensities of Raman intrinsic modes are only detected for ^{70}Ge coverage $\theta \geq 0.6$ ML. Figure 2(a) shows Ge-Ge modes of all-^{76}Ge, all-^{70}Ge, and ^{70}Ge/^{76}Ge islands grown by depositing 0.6 ML on the 2D layer. We note that the Ge-Ge mode of ^{70}Ge/^{76}Ge islands is strikingly closer to the ^{76}Ge-^{76}Ge peak than the ^{70}Ge-^{70}Ge peak, demonstrating a strong flow of ^{76}Ge from the 2D layer during the islanding process. This corresponds to $y(0.6 \text{ ML}) = 0.886$, which signifies that roughly 90% of Ge atoms within the grown islands are actually atoms initially deposited during the planar growth, and direct beam atoms count for only $\sim$10%. The strong Ge diffusion from the 2D metastable layer takes place because the nucleated islands are energetically more favorable bonding sites. Earlier studies have reported the thinning of the 2D layer following the onset of the 3D growth [13–16,19]. Extensive STM investigations have demonstrated the etching of the 2D layer upon islanding [16]. Schülli *et al.* have suggested that $\sim$1 ML is depleted from the 2D layer at a growth temperature of 500 °C [19]. A similar reduction of the thickness of the layer between the growing islands was also inferred from photoluminescence studies [13,14] and selective chemical etching [15]. The use of stable isotope tracing presented here allows the quantification of this Ge surface transport during the islanding process, in addition to the identification of the origin of Ge atoms incorporated into the growing islands.

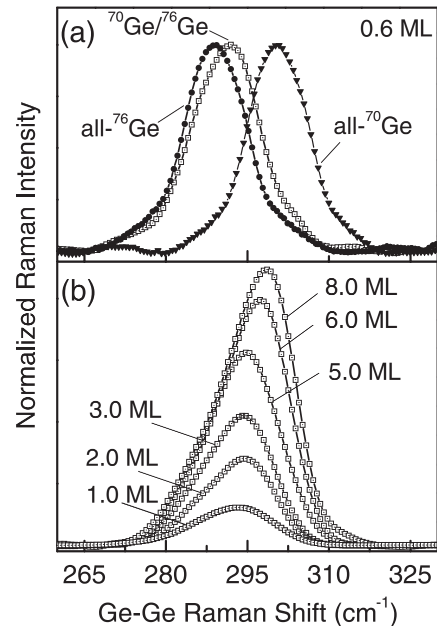

FIG. 2. (a) Ge-Ge LO phonon of Ge/Si(001) islands grown by deposition of 0.6 ML on the 2D layer using the enriched sources ^{76}Ge (all ^{76}Ge) and ^{70}Ge (all ^{70}Ge), and the two-isotope approach (^{70}Ge/^{76}Ge). (b) Ge-Ge Raman peak of ^{70}Ge/^{76}Ge islands recorded at different amounts of ^{70}Ge deposited on the planar 4.4 ML-thick ^{76}Ge layer. The asymmetric broadening of Ge-Ge modes can be associated with an inhomogeneous distribution of ^{70}Ge and ^{76}Ge within the islands.

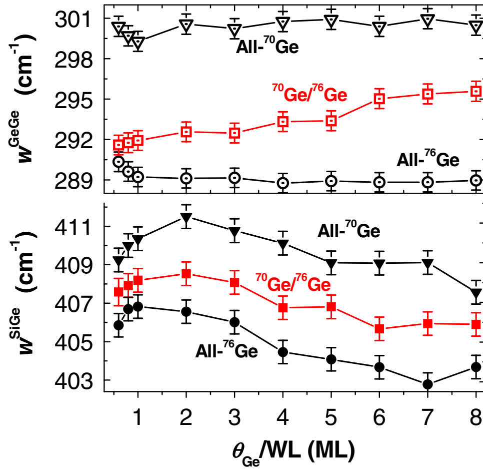

FIG. 3 (color online). The evolution as a function of θ of Ge-Ge (top panel) and Si-Ge (bottom panel) wave numbers for the three varieties of the grown islands investigated in this study. Each data point represents the average over several measurements.

The investigated islands are predominantly faceted domes, as demonstrated by AFM and transmission electron microscopy analyses (not shown). The islands reach their steady state density at $\theta = 1$ ML [21]. The Ge-Ge LO phonon spectra of ^{70}Ge/^{76}Ge islands grown by deposition of different amounts of ^{70}Ge ($\theta \geq 1$ ML corresponding to the growth stage) are shown in Fig. 2(b). The observed enhancement in Raman intensity with θ comes from the increase in island volume. The important feature here is the gradual upshift of Ge-Ge modes suggestive of an increase in the content of direct beam atoms (^{70}Ge) within the growing islands. It is important to mention that these islands also contain Si atoms. We found that the Si content, as estimated from Raman data [24], decreases slightly from $\sim$32% to $\sim$25% by increasing ^{70}Ge coverage from 0.6 to 8 ML. The relative variation is $\sim$2.5% in the reduced mass resulting from Ge isotope substitution in the Si-Ge system, which translates into a $\sim$3 cm^{-1} shift between Si-^{70}Ge and Si-^{76}Ge Raman peaks (compared to a $\sim$11.8 cm^{-1} shift between ^{76}Ge-^{76}Ge and ^{70}Ge-^{70}Ge). Thus one can expect the quantification of Ge transport from the evolution of the Si-Ge mode to be fraught with large errors and to be less sensitive. Therefore, we restrict our analysis to the Ge-Ge mode. Nevertheless, it is worth pointing out that the Si-Ge mode in ^{70}Ge/^{76}Ge islands remains practically in between the Si-^{70}Ge and Si-^{76}Ge modes (Fig. 3), which drives us to conclude, within the accuracy of our setup, that Si is equally mixed with both isotopes in ^{70}Ge/^{76}Ge islands. Figure 3 also displays the evolution of the average position of the Ge-Ge peak in ^{70}Ge/^{76}Ge islands, which is found to shift monotonically with the coverage to higher wave numbers but remains $\sim$5 cm^{-1} below the ^{70}Ge-^{70}Ge mode at the highest deposited amount of ^{70}Ge ($\theta =$ 8 ML). Our analysis is limited to the coverage range $\theta \leq$ 8 ML because the deposition of more than 8 ML yields superdome islands, which can affect the accuracy of our analysis.

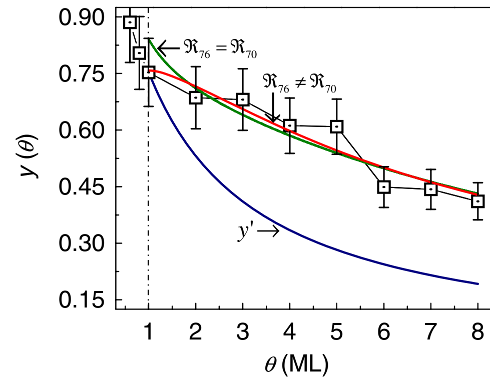

FIG. 4 (color online). The evolution of y as a function of the amount of Ge deposited on the 2D layer (squares). Lines show the fits using the equations described in the text. The vertical dashed line denotes the end of the nucleation stage.

Figure 4 displays the evolution of y as a function of θ. We note that at the end of the nucleation stage ($\theta = 1$ ML) ^{76}Ge atoms initially deposited during the planar growth count for about $\sim$75% of Ge atoms within the islands. This fraction, however, diminishes progressively with the additional evaporation of ^{70}Ge to reach $\sim$41% at $\theta = 8$ ML. This decrease occurs at the expense of the increasing incorporation of direct beam atoms (^{70}Ge) into the growing islands. If we assume that during the growth regime ($\theta \geq$ 1 ML) *only* and *all* direct beam ^{70}Ge atoms contribute to the growth, the fraction of ^{76}Ge within the island can be expressed as $y' = \wp_{76}^{\rm nucl}/(\wp_{76}^{\rm nucl} + \wp_{70}^{\rm nucl} + \theta')$, where $\wp_{76}^{\rm nucl}$ and $\wp_{70}^{\rm nucl}$ represent the amounts (in ML) of ^{76}Ge and ^{70}Ge transferred to 3D islands during the nucleation stage, respectively. θ' is the additional amount of ^{70}Ge deposited during the growth stage ($\theta' = \theta - 1$ ML). The calculated values of y' are also shown in Fig. 4. It is clear that the assumption made above leads to an important underestimation of the amount of ^{76}Ge in the islands. Obviously, other subtle factors must be taken into account. In general, the 3D growth involves several kinetically driven processes, including (1) ^{70}Ge atom adsorption to the growing surface; (2) formation of adatoms (the only mobile surface species) responsible for mass transport on the surface of the 2D layer; (3) diffusion and hopping between surface sites; and (4) capture of adatoms (adatom attachment and diffusion on island facets). Ge desorption and detachment from the islands are negligible under our experimental conditions. Thus a more realistic description of the mass transport during the growth should consider that impinging beam atoms (^{70}Ge) contribute only partially to the 3D growth and that ^{76}Ge atoms continue flowing from the 2D layer towards the islands. In general, the fraction of ^{76}Ge within the island can be expressed as

$$y(\theta') = \frac{\wp_{76}^{\rm nucl} + \wp_{76}^{\rm grow}(\theta')}{(\wp_{76}^{\rm nucl} + \wp_{70}^{\rm nucl}) + \wp_{76}^{\rm grow}(\theta') + \wp_{70}^{\rm grow}(\theta')}, \quad (1)$$

where $\wp_{76}^{\text{grow}}$ and $\wp_{70}^{\text{grow}}$ are the amount of ^{76}Ge and ^{70}Ge atoms transferred to the island during the growth regime, respectively. Assuming that ^{70}Ge atoms from the direct beam induce only a small perturbation on the areal density of adatoms [27], the island growth rate is given by $\Re_{76} \times \wp_{76}^{2D} + (\Re_{70} \times \wp_{70}^{2D} + \rho \times A)$. The constant rates $\Re_{70}$ and $\Re_{76}$ are related to attempt frequencies and effective activation barriers by $\Re_i = \Re_i^0 \exp(-E_a^i/kT)$ (i denotes 70 or 76). k is Boltzmann's constant. A is the relative area covered by islands, and the term $\rho \times A$ counts for the rate of ^{70}Ge falling directly on the growing island. In the investigated coverage range, A varies over the 0.22–0.3 range. $\wp_{76}^{2D} = \theta_0 - \wp_{76}^{\text{nucl}} - \wp_{76}^{\text{grow}}$ and $\wp_{70}^{2D} = \theta \times (1 - A) - \wp_{70}^{\text{nucl}} - \wp_{70}^{\text{grow}}$ are the amounts of ^{76}Ge and ^{70}Ge available in the 2D layer. From this, the evolution of $\wp_{76}^{\text{grow}}$ and $\wp_{70}^{\text{grow}}$ can be described by the following rate equations:

$$\frac{d\wp_{76}^{\text{grow}}}{dt} = \Re_{76} \times (\theta_0 - \wp_{76}^{\text{nucl}} - \wp_{76}^{\text{grow}}), \tag{2}$$

$$\frac{d\wp_{70}^{\text{grow}}}{dt} = \rho \times A + \Re_{70} \times (\theta \times (1 - A) - \wp_{70}^{\text{nucl}} - \wp_{70}^{\text{grow}}). \tag{3}$$

Assuming an identical behavior of ^{70}Ge and ^{76}Ge atoms on the 2D layer (i.e., $\Re_{76} = \Re_{70}$), a good fit of the experimental data gives an effective activation energy $E_a^{76} = E_a^{70} \approx 2.56$ eV for a fixed attempt frequency $\Re_{70}^0 = \Re_{76}^0 = 5 \times 10^{12}$ s^{-1} (Fig. 4). The fit is not sensitive to A, which was kept constant at 0.25. The best fit, however, is obtained using two different activation energies, $E_a^{76} \approx$ 2.51 eV and $E_a^{70} \approx 2.71$ eV (Fig. 4). Considering the accuracy of our analysis, it is hard to conclude if this difference is meaningful. It is important to mention that the obtained effective energies represent the ensemble of kinetic barriers involved in the growth of Ge/Si 3D nanostructures using solid source molecular beam epitaxy. The determination of the individual energetic barriers involved in this strain-mediated self-assembly remains, however, an open challenge. Based on mean-field theory, an attempt was made to estimate these quantities by fitting the density of InP/GaAs islands (a system with a close lattice mismatch to Ge/Si) grown by metalorganic vapor phase epitaxy in the temperature range of 580–640 °C [28]. The total of the calculated activation energies was found to be ~2.18 eV [28], which is below the values obtained in this work despite the fact that the metalorganic vapor phase epitaxy growth would require an additional barrier due to the presence of reaction products at the surface [29]. The use of six adjustable parameters, however, can possibly project an important uncertainty on the calculated energies [28]. Finally, the calculated values of $\wp_{76}^{2D}$ and $\wp_{70}^{2D}$ indicate that the total amount of Ge in the 2D layer drops from the initial 4.4 ML to ~1.3 ML at the end of the nucleation stage ($\theta = 1$ ML). This amount increases nearly linearly during the growth stage to reach ~3.2 ML at $\theta = 8$ ML.

To conclude, we have presented a novel approach to address the transport of Ge deposited atoms during strain-mediated self-assembly. Through Ge stable isotope tracing and Raman analysis of the Ge-Ge LO phonon, we have demonstrated that the islands contain an important fraction of Ge atoms initially deposited during the planar growth indicating a strong transfer of Ge from the 2D metastable layer, whereas direct beam atoms deposited at and after the onset of the 3D growth contribute only partially to the growing islands. The quantification of the Ge flow was obtained within the harmonic approximation of Ge-Ge vibrations and described using a rate equation model.

O. M. is grateful to Jerry Tersoff for fruitful discussions and to JSPS for financial support. The authors are thankful to Oscar D. Dubon and Kin Man Yu for RBS measurements. This work was supported in part by a Grant-in-Aid for Scientific Research No 18001002, in part by Special Coordination Funds for Promoting Science and Technology, and in part by a Grant-in-Aid for the Global Center of Excellence at Keio University.

*moutanab@mpi-halle.mpg.de

[1] D. J. Eaglesham and M. Cerullo, Phys. Rev. Lett. **64**, 1943 (1990).
[2] Y.-W. Mo *et al.*, Phys. Rev. Lett. **65**, 1020 (1990).
[3] J. Stangl, V. Holý, and G. Bauer, Rev. Mod. Phys. **76**, 725 (2004).
[4] Y. Tu and J. Tersoff, Phys. Rev. Lett. **98**, 096103 (2007).
[5] Z.-F. Huang and K. R. Elder, Phys. Rev. Lett. **101**, 158701 (2008).
[6] I. Berbezier and A. Ronda, Surf. Sci. Rep. **64**, 47 (2009).
[7] K. L. Man *et al.*, Phys. Rev. Lett. **101**, 226102 (2008).
[8] T. Walther *et al.*, Phys. Rev. Lett. **86**, 2381 (2001).
[9] Y. Tu and J. Tersoff, Phys. Rev. Lett. **93**, 216101 (2004).
[10] J. Tersoff, Phys. Rev. Lett. **74**, 5080 (1995).
[11] C. W. Snyder *et al.*, Phys. Rev. Lett. **66**, 3032 (1991).
[12] D. Leonard *et al.*, Phys. Rev. B **50**, 11687 (1994).
[13] P. Schittenhelm *et al.*, Appl. Phys. Lett. **67**, 1292 (1995).
[14] V. Le Thanh, Surf. Sci. **492**, 255 (2001).
[15] U. Denker *et al.*, Appl. Phys. Lett. **78**, 3723 (2001).
[16] B. Voigtländer, Surf. Sci. Rep. **43**, 127 (2001).
[17] T. Schwarz-Selinger *et al.*, Phys. Rev. B **65**, 125317 (2002).
[18] U. Denker *et al.*, Phys. Rev. Lett. **94**, 216103 (2005).
[19] T. U. Schülli *et al.*, Appl. Phys. Lett. **89**, 143114 (2006).
[20] M. S. Leite *et al.*, Phys. Rev. Lett. **100**, 226101 (2008).
[21] S. Miyamoto *et al.*, Phys. Rev. B **79**, 165415 (2009).
[22] M. Born and K. Huang, *Dynamical Theory of Crystal Lattices* (Clarendon Press, Oxford, United Kingdom, 1954).
[23] M. Brehm *et al.*, Phys. Rev. B **80**, 205321 (2009).
[24] P. H. Tan *et al.*, Phys. Rev. B **68**, 125302 (2003).
[25] O. Moutanabbir *et al.*, J. Cryst. Growth **301–302**, 324 (2007).
[26] M. Cardona and M. L. W. Thewalt, Rev. Mod. Phys. **77**, 1173 (2005).
[27] R. M. Tromp and M. Mankos, Phys. Rev. Lett. **81**, 1050 (1998).
[28] H. T. Dobbs *et al.*, Phys. Rev. Lett. **79**, 897 (1997).
[29] D. Kandel, Phys. Rev. Lett. **78**, 499 (1997).